Journal of Non-Crystalline Solids 355 (2009) 1508–1516

Contents lists available at ScienceDirect

Journal of Non-Crystalline Solids

journal homepage: www.elsevier.com/locate/jnoncrysol

Amorphous to crystalline transition and optoelectronic properties of nanocrystalline indium tin oxide (ITO) films sputtered with high rf power at room temperature

V. Malathy [a], S. Sivaranjani [b], V.S. Vidhya [c], J. Joseph Prince [d], T. Balasubramanian [a], C. Sanjeeviraja [b], M. Jayachandran [c,*]

[a] Department of Physics, National Institute of Technology, Trichy-620 015, India
[b] Department of Physics, Alagappa University, Karaikudi-630 003, India
[c] ECMS Division, Central Electrochemical Research Institute, Karaikudi-630 006, India
[d] Department of Physics, Anna University, Trichy-620 024, India

ARTICLE INFO

Article history:
Received 11 December 2008
Received in revised form 20 April 2009
Available online 29 June 2009

PACS:
81.07.Bc
71.20.Nr
81.15.Cd
91.05.Cp
78.66.W
73.61.r

Keywords:
UPS/XPS
X-ray diffraction
Conductivity
Sputtering
Optical spectroscopy
Atomic force and scanning tunneling microscopy

ABSTRACT

ITO thin films were deposited on quartz substrates by the rf sputtering technique using various rf power keeping the substrates at room temperature. The influence of rf power on the structural, electrical, optical and morphological properties was studied by varying the rf power in the range 50–350 W. X-ray diffraction results show an amorphous – crystalline transition with nano grains. At a power of 250 W, the ITO film showed preferential orientation along (4 0 0) peak. It is observed from the optical transmission studies that the optical band gap increased from 3.57 to 3.69 eV when the rf power was increased from 50 to 250 W. The resistivity value is minimum and grain size is maximum for the ITO film deposited at 250 W. The X-ray photoelectron spectroscopy (XPS), Energy dispersive X-ray (EDX) and Atomic force microscopy AFM results confirm that the ITO films are stoichiometric and the surface contained nano-sized grains distributed uniformly all over the surface. It can be concluded that the ITO film deposited at room temperature with 250 W rf power, can provide the required optical and electrical properties useful for developing optoelectronic devices at lower temperatures.

© 2009 Published by Elsevier B.V.

1. Introduction

Thin films of transparent conducting oxide (TCO) have attracted greater attention due to their interest optoelectronic properties of high optical transparency in the visible wavelength region associated with low sheet resistance [1]. This unique combination makes TCO films highly relevant to various applications and in developing optoelectronic and electronic devices [2]. Among the many available TCOs, ITO is the most frequently used material, both amorphous and crystalline form, in developing practical optical and electronic devices [3].

Indium tin oxides films have been deposited containing Sn^{4+} ions hosted in the In_2O_3 structure with concentrations varying up to 15% [4]. ITO is a highly degenerate n-type semiconductor with a wide band gap (3.5–4.3 eV), having low enough electrical resistivity of about $10^{-4}\ \Omega$ cm making it easy to be interfaced with electronic circuits and simultaneously shows high transmission in the visible and near infrared (NIR) regions of the electromagnetic spectrum [5]. Its low electrical resistivity results from either the non-stoichiometry produced by oxygen deficiency or by the incorporation of tin as tetravalent dopant or from both [6]. Moreover, ITO exhibits excellent substrate adherence, hardness, and chemical inertness. Because of these advantageous physico-chemical properties ITO is widely used as transparent electrodes for optoelectronic devices such as solar cells [7], flat panel displays [8], electro chromic devices [1], energy efficient windows, heat reflecting mirrors and anti-reflection coatings [9] in addition to gas sensors [10].

The properties of ITO films such as electrical resistivity, optical transmittance, sensitivity to toxic gases are found to strongly

* Corresponding author. Tel.: +91 04565 227555x218; fax: +91 04565 227713.
E-mail address: jayam54@yahoo.com (M. Jayachandran).

0022-3093/$ - see front matter © 2009 Published by Elsevier B.V.
doi:10.1016/j.jnoncrysol.2009.04.043

depend on the deposition condition, and also due to their acquired structural, morphological and compositional nature [11]. Out of many preparation techniques including thermal/electron beam evaporation, rf/dc sputtering, pulsed laser deposition, chemical vapor deposition, sol–gel process, spray pyrolysis, spin/dip coating process, rf sputtering process has emerged as the most viable technique for depositing device quality and large area ITO thin film [12].

Most of the above techniques require high temperature (300–550 °C) during deposition to obtain crystalline ITO films, and also some times a high temperature post-deposition annealing treatment (400–650 °C) to improve crystallinity or orientation which generally damage the film surface and substrate properties during device development. As far as thin films production by sputtering technique is concerned, the rate of deposition, substrate temperature and the rf power are perhaps the most critical parameters which determine their materials properties and quality. Dependence of the optoelectronic properties of sputter deposited ITO films at 250 °C by using low rf power has been reported [13]. Hence, a study of ITO films sputter deposited at room temperature using high rf power, is felt very important which is highly required to develop optoelectronic devices at a relatively low temperature of less than 150 °C. Therefore, to optimize the growth parameters, in order to deposite the films reproducibly and to facilitate the fabrication of devices, a detailed study of the impact of high rf power on the structural, optical, electrical and morphological properties of ITO films deposited at room temperature, without involving a high temperature post-deposition treatment have been carried out. Further, only few reports are available on the change of preferred orientation of crystallites in ITO films with various rf sputtering deposition conditions [14–16]. However, the mechanism of orientation change has not yet fully understood. It is important to unravel the basic mechanism associated with the development of preferential orientation in ITO films, because the crucial materials properties like optical transmittance, grain size variation, lattice parameters and surface morphology are highly dependent on preferential orientation. In this study, we present the results on the orientation development mechanism of ITO films at room temperature and its dependence on rf sputtering power.

.

2. Experiment

ITO films were deposited on quartz substrates at room temperature using 13.56 MHz radio frequency magnetron sputtering system with 99.99% tin doped indium oxide (90:10 at%) ceramic target (5 cm diameter, 5 mm thickness) in argon atmosphere without the addition of oxygen. The quartz substrates (1 cm x 1 cm) were first cleaned by a detergent, washed with distilled water, kept in freshly prepared hot chromic acid for 1 h, again thoroughly cleaned with distilled water and finally subjected to ultrasonic cleaning for 1 h. It was observed that the substrate temperature goes to a minimum of about 40 °C only when the substrate was placed at larger distance above the target, sputtering was carried out by keeping the target to substrate distance constant at about 8 cm through out the experiment. Temperature of the substrate was maintained at room temperature and controlled through out the deposition process by mounting on water-cooled substrate table. A thermo couple was used to measure and control the temperature of the water-cooled substrate table. The base pressure in chamber was 10^{-6} Torr and the argon pressure was maintained at 5×10^{-3} Torr. The rf power was varied between 50 and 350 W in steps of 50 W and the deposition was carried out for 20–30 min. Film thickness was maintained in the range 450–500 nm by adjusting the time as measured by the Stylus Profilometer (Mitutoyo). The optical transmittance measurements were made in the wavelength range 300–2500 nm using a Hitatchi-330 UV–vis-NIR spectrophotometer. X-ray diffraction (XRD) measurements were carried out with X'pert Pro PANalytical-3040 using CuKα radiation (λ = 1.5406 Å) to study the crystalline properties of the films. Electrical properties were measured by the four-probe method with a Four probe setup model DFP-02 (Scientific Equipment) dc power supply. Hall mobility and carrier concentration were calculated from the Hall voltage measured by Vander Pauw method with a Ecopia HMS 3000 Hall constant measurement system. The elemental composition of the film was analyzed using an energy-dispersive X-ray (EDX) spectrometer attached with the JEOL JSM-35 CF SEM instrument. The surface morphology and surface roughness of the films were investigated using a Nanoscope E-3138j AFM/STM Atomic force microscope (AFM). Mean roughness of the deposited films are determined on a scan area of 3×3 µm. Analysis of chemical state of elements was achieved using a Multilab 2000 X-ray photoelectron spectroscope (XPS) with MgKα (1253.6 eV) X-ray source. The XPS spectra were scanned in the binding energy range of 0–1100 eV. The carbon 1s peak position was fixed as the standard with a binding energy of 287.0 eV to compensate the observed charge-induced shifts. The spectrometer resolution was fixed at 1 eV for wide scan and 0.05 eV for narrow scan.

3. Results

3.1. Effect of rf power on the structure of the films

The hump centered at about 25° in Fig. 1(a) and (b) indicates the formation of amorphous ITO films at rf power 50 and 100 W which clearly shows their non-crystalline amorphous nature. For the films deposited using 150 and 200 W power as shown in Fig. 1(c) and (d), respectively, the emergence of a peak at 30.58° embedded within a hump around this region and another peak at about 51° shows that the films have mixed amorphous and crystalline phase with (2 2 2) and (4 0 0) diffraction peaks of In_2O_3 cubic crystalline structure. This may be due to the fact that the kinetic energy of low mobility atoms or particles on the substrate

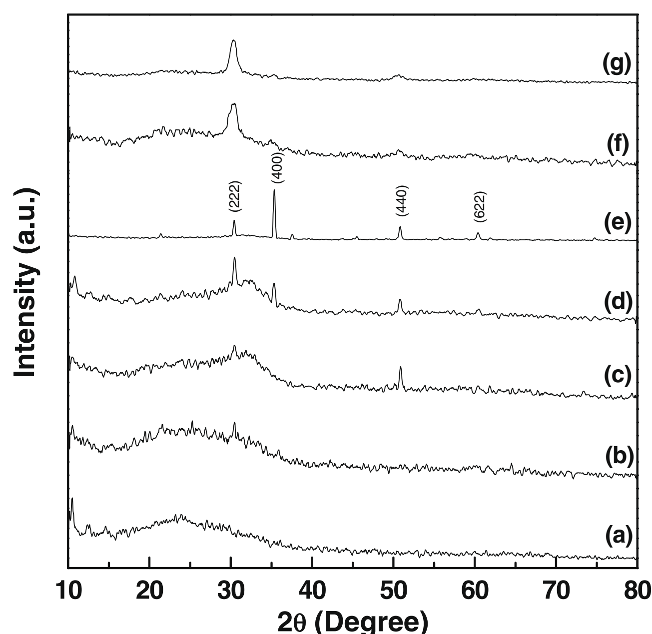

Fig. 1. XRD patterns of ITO thin films rf sputtered using various rf power: (a) 50 W, (b) 100 W, (c) 150 W, (d) 200 W, (e) 250 W, (f) 300 W and (g) 350 W.

was not sufficient enough to effect a complete amorphous to crystalline phase transition [17], but partially. At 250 W, complete transformation to highly crystalline structure is observed as evident from the XRD spectra (Fig. 1(e)) in which (4 0 0) preferential orientation is indicated. But, ITO films deposited with rf power greater than 300 W show less crystalline nature and reduced grain size as can be explicitly seen from the presence of broadened peak at $2\theta = 30.8^{o}$ corresponding to (2 2 2) peak. All the ITO films deposited between 150 and 350 W showed a peak at $2\theta = 30.85^{o}$, which corresponds to (2 2 2) plane of $In_{1.88}Sn_{0.12}O_3$ crystalline film [JCPDS card No. 89-4598]. This is due to the greater kinetic energy of several electron volts acquired by the sputtered particles at high rf power. None of the XRD spectra showed any characteristic peaks of Sn, SnO and SnO_2, which confirms that tin atoms were doped substitutionally in the In_2O_3 lattice [18]. It is obvious that the main conduction mechanism of ITO films deposited at low rf power is due to the formation of oxygen vacancies, which provide two electrons for each vacancy [19]. In the present case, when the ITO film is amorphous, some of these electrons are trapped in short range by the net non-crystalline as well as non-uniform structure. At 250 W, when the structure of the film becomes highly crystalline and oriented, these trapped electrons will be released from the traps. Thus, the larger mobility, higher carrier concentration and low resistivity observed, as will be discussed later, for the ITO films deposited with 250 W may be attributed to the lattice transition effected near the amorphous-crystalline transition region [20] and the development of (4 0 0) preferred orientation.

The lattice parameter (a) was determined for cubic structure by the following expression:

$$a = d\sqrt{h^2 + k^2 + l^2}, \tag{1}$$

where h,k,l are the Miller indices of the lattice plane.

The grain size (D) was calculated using the Scherrer formula from the full-width at half maximum (FWHM) (β)

$$D = \frac{0.94\lambda}{\beta\cos\theta}, \tag{2}$$

where λ is the wavelength of the X–ray used, θ is the Bragg diffraction angle and β is the FWHM in radian.

Fig. 2 shows the change of lattice parameter and grain size values with rf power. The grain size is found increasing with rf power up to 250 W and then shows a decreasing trend. This behavior shows that crystallinity of the films increases from amorphous nature at 50 W as observed from the sharp XRD peaks. The decrease in grain size at 300 W as evident from the broader (2 2 2) peak shows the degradation in crystallinity at above the critical higher rf power. In the present study, this critical rf power is 250 W where highest crystallinity is observed for the ITO films. The lattice constant value of ITO films decreases from 50 to 250 W and then increases. However, the minimum 'a' value at 250 W 10.120 Å which is larger than that for undoped In_2O_3 (10.118 Å).

3.2. Effect of rf power on the microstructural parameters

Effect of rf power on the micro structural parameters of the ITO were also studied. The values of strain (ε), dislocation density (δ) and number of crystallites (N) were calculated using the standard formulae [12], for the ITO films with the lattice reflection planes (2 2 2).

The strain value ε can be evaluated by using the following relation:

$$\varepsilon = \left(\frac{\lambda}{D\cos\theta}\right) - \left(\frac{\beta}{\tan\theta}\right), \tag{3}$$

The dislocation density (δ) has been calculated by using the formula for thin films with cubic structure:

$$\delta = \frac{15\varepsilon}{aD}, \tag{4}$$

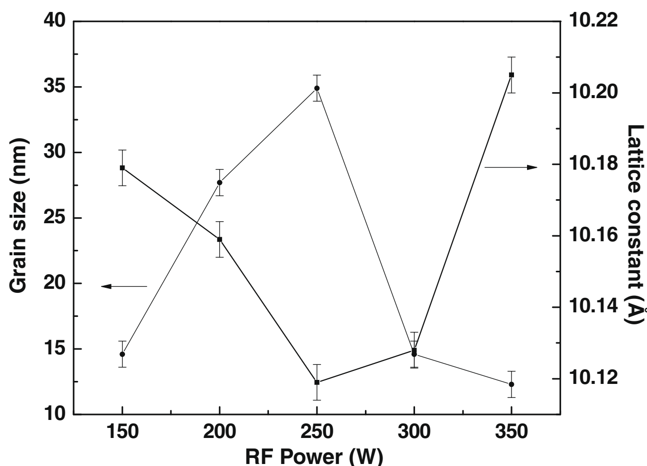

Fig. 2. Variation of grain size (D) and lattice constant (a) of ITO films deposited with different rf power.

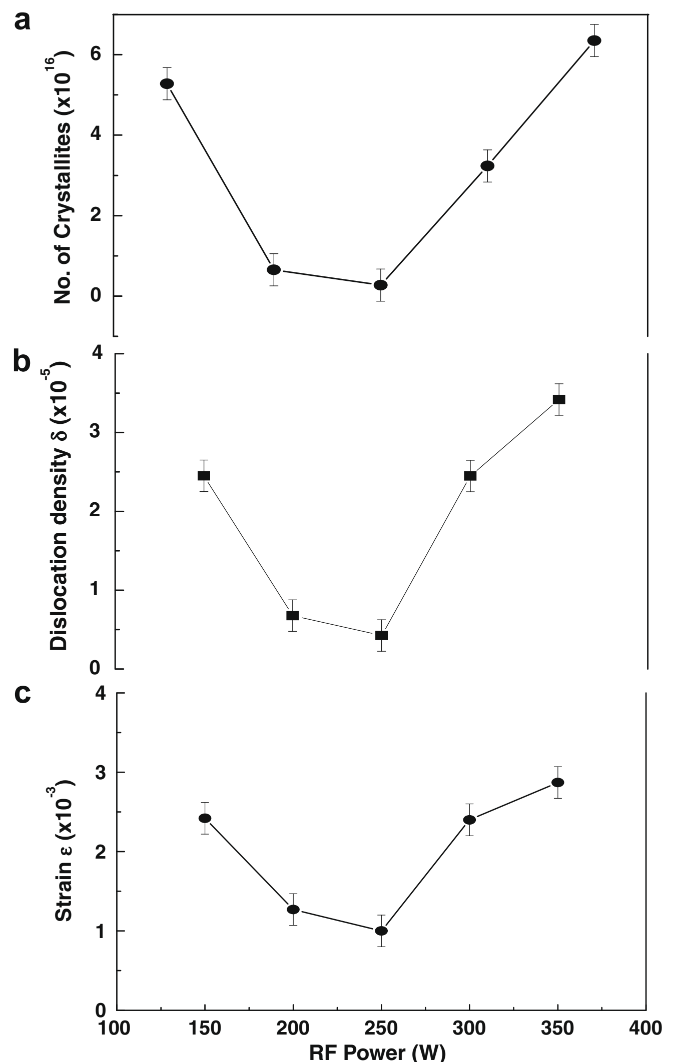

Fig. 3. Dependence of microstructural parameters: (a) strain, (b) dislocation density and (c) number of crystallites of ITO films deposited at different rf power.

Using grain size (D) and film thickness (t), the number of crystallites N can be estimated using the relation:

$$N = \frac{t}{D^3} / \text{ unit area}, \quad (5)$$

These microstructural parameters for the ITO thin films deposited with different values of rf power 150–350 W are shown in Fig. 3(a–c), in which a minimum value for each of them is observed at 250 W.

3.3. Optical studies

Optical transmission spectra were recorded for ITO films deposited at sputtering powers varying from 50–350 W. Fig. 4 shows the representative transmittance spectra of ITO films deposited at 50, 250 and 350 W, respectively. The transmittance data obtained for the films were used to calculate the absorption coefficient (α) at different wavelengths using the following relation:

$$T = \exp(-\alpha t), \quad (6)$$

where t is the film thickness and T is the transmittance of the film at a particular wavelength. The optical band gap E_g, can be estimated from the Tauc plot drawn using the relation:

$$\alpha h\nu = A(h\nu - E_g)^\gamma, \quad (7)$$

where A is a constant, υ is the transition frequency and the exponent γ characterizes the nature of band transition between the valence band and the conduction band. The band gap can be obtained from extrapolation of the straight-line portion of the $(\alpha h\upsilon)^\gamma$ vs $h\upsilon$ plot to $\alpha = 0$ as shown in the inset of Fig. 4 for the ITO film deposited at 250 W. It is observed that for all the ITO films, the best straight line fit is obtained for γ equal to 1/2, which is expected for direct allowed transition [21].

The dependence of optical band gap of ITO films on rf power is shown in Fig. 5. The optical band gap of ITO films first increased with rf power, reaching maximum a value of 3.69 eV at 250 W and then decreased. The increase in band gap from 3.57 to 3.69 eV can be explained on the basis of Burstein-Moss effect [22] which is directly proportional to carrier concentration of a semiconductor film. The increase in carrier concentration influences the conduction band gap widening. At 350 W power, the deposited ITO films has a lower band gap value of 3.30 eV which is consistent with the observed reduced carrier concentration of this film.

Refractive index (n) and extinction coefficient (k) values of ITO films in the wavelength range 350–1000 nm were calculated from the interference patterns of transmission spectra [23]. The method used to determine the optical constants of thin films based on the measurements of intensity of transmitted light [23–25] was used to develop a computer program to calculate n and k values. Explicit expressions for n and k were derived from the fringe pattern of transmission spectrum of a thin transparent film assumed to be surrounded by non-absorbing media. The maxima and minima from transmission spectra of the transparent film were used for the computation. Fig. 6 shows the variation of n and extinction coefficient with wavelength for the film deposited at 250 W. It shows a higher refractive index value of 1.88 at 550 nm which is in good agreement with the reported value 1.86 for the ITO films deposited by reactive rf magnetron sputtering [26]. The average extinction coefficient value is about 0.05. It confirms the formation of highly compact, void free and fully crystallized structure of the ITO films deposited under the optimized conditions observed in the present study.

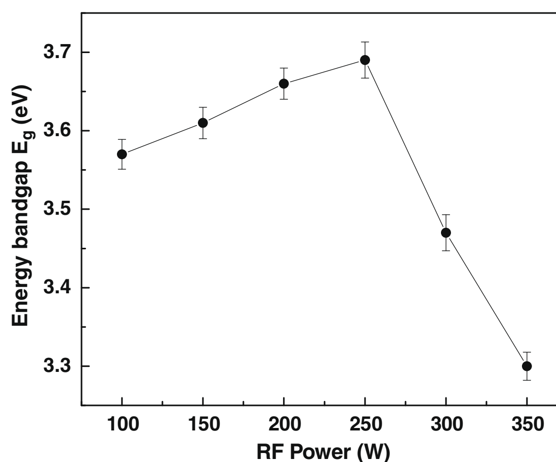

Fig. 5. Variation of optical band gap with rf power for ITO films deposited at room temperature.

3.4. Electrical properties

Fig. 7 shows the resistivity and the sheet resistance as a function of rf power. It is observed that the sheet resistance (R_s) decreases with increasing rf power, the minimum sheet resistance achieved is about 26.5 Ω/square for the ITO film deposited with

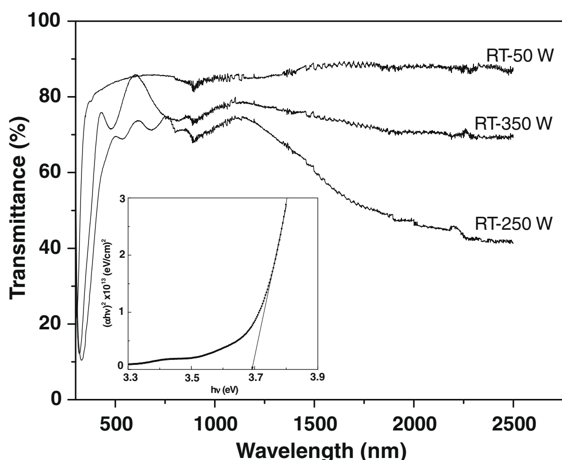

Fig. 4. Optical transmission spectra of ITO films deposited at various rf power and inset showing $(\alpha h\nu)^2$ vs $h\nu$ curve for the ITO film deposited at 250 W.

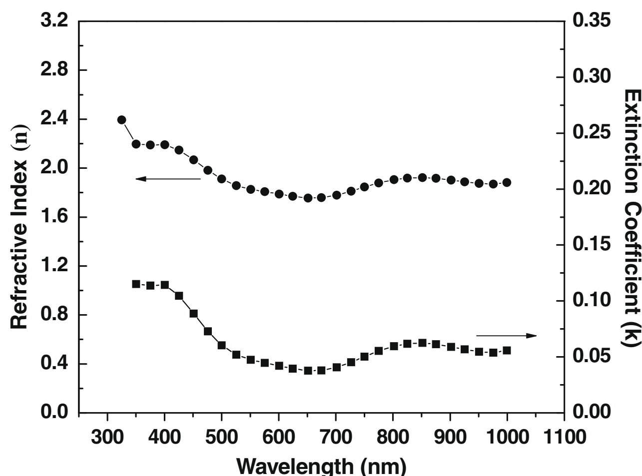

Fig. 6. Variation of refractive index and extinction coefficient with wavelength for the ITO film deposited using 250 W at room temperature.

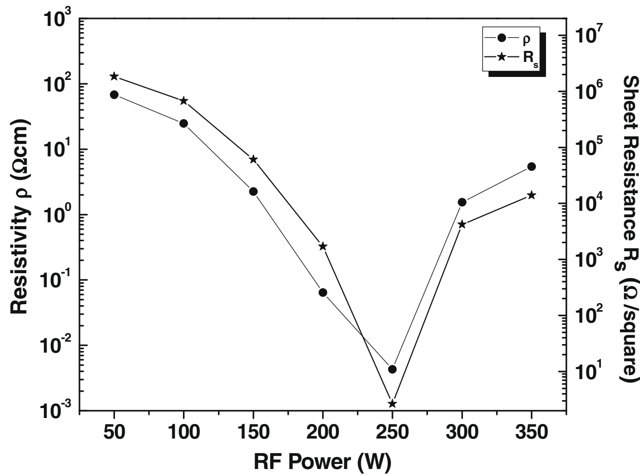

Fig. 7. Dependence of resistivity ρ and sheet resistance R_s on rf power.

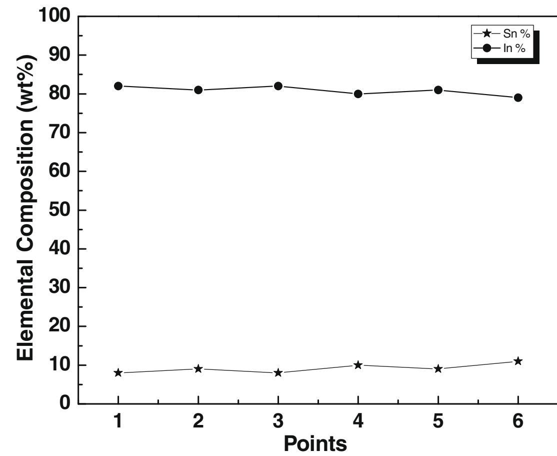

Fig. 9. Variation of In and Sn concentration at different points on the surface of ITO film deposited with 250 W at room temperature.

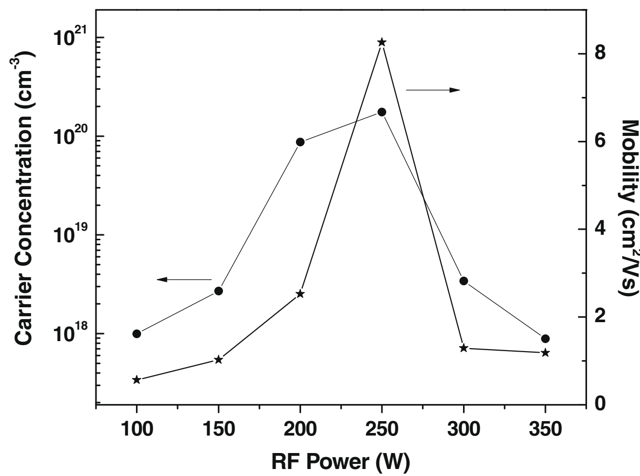

Fig. 8. Carrier concentration (n) and mobility (μ) of ITO films deposited at various rf power.

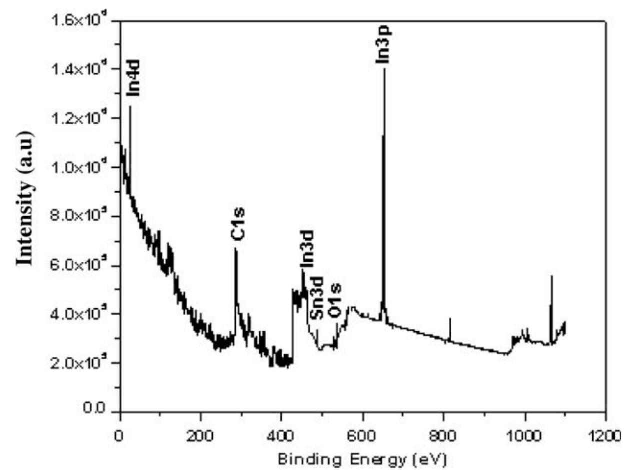

Fig. 10. XPS scan of ITO film deposited at 250 W.

250 W power. Then an increase in R_s values is seen. Similarly, the resistivity value of ITO film also shows the same trend, with a minimum resistivity value of 4.3×10^{-3} Ω cm at 250 W and larger resistivity values on both higher and lower rf power regions. In order to achieve low resistivity in ITO films, there is a trade off between their resistivity and the corresponding carrier concentration/mobility.

The semiconducting and electronic properties show an excellent dependence on the rf power and consequently on the crystalline quality of the ITO films. Fig. 8 shows the variation of carrier concentration (n) and mobility (μ) with rf power. Highest mobility value is observed for the ITO films deposited at 250 W which also shows the lowest resistivity with the presence of maximum carrier concentration of 1.75×10^{20} cm^{-3} confirming the degenerate nature of this ITO film. The recorded carrier concentration values show a variation of about 10^{18}–10^{20} cm^{-3} for the ITO films deposited at 100 and 250 W, respectively. This shows the transformation of amorphous ITO films formed at rf power less than 100 W to well crystallized films at 250 W.

These electrical properties show that ITO films with amorphous nature are formed for rf power less that 100 W. On increasing the power, the crystalline nature increases gradually and attains maximum crystallinity at an rf power of 250 W. Beyond this rf power, the deposited ITO film shows a reduced value of carrier concentration exposing a deteriorated crystalline nature. The lowest resistivity value observed for the ITO films deposited at 250 W is in accordance with the trend seen for the carrier concentration. An increase in mobility is observed with increasing rf power which became maximum at 250 W and then decreased on further increase of power, up to 350 W.

3.5. Microstructure and surface morphology studies

All the deposited films were highly transparent in the visible region and uniform over the entire surface. The elemental composition ratio of Sn to In was analyzed by EDX. This study was conducted by selecting six different points on the surface of ITO films deposited at 250 W to investigate the dopant distribution of Sn in the ITO lattice. Since uniform distribution of dopants is very essential in nanocrystalline films, the dopants should be exactly incorporated into the matrix to the maximum extent possible. If this is not achieved, segregated doping occurs leading to the presence of separated In_2O_3 and SnO_2 particles which will degrade the optical and electrical properties of ITO films rendering them not useful in optoelectronic devices [27]. Fig. 9 shows the EDX analysis at various points on the ITO films deposited at 250 W rf power. The distribution of Sn is observed in the range of 8–11 wt% and that of In about 79–82 wt% with in the deviation

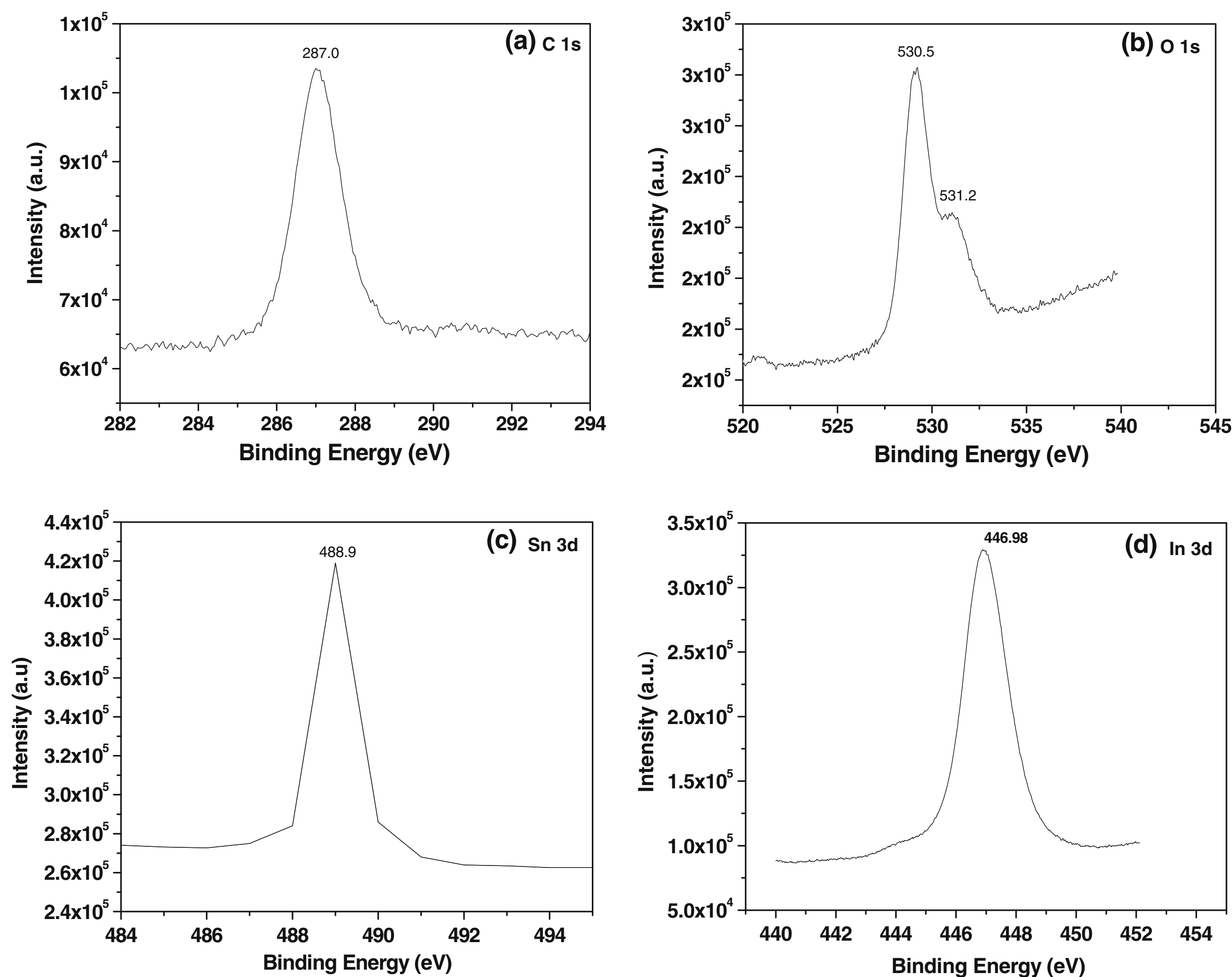

Fig. 11. XPS narrow scans of ITO film deposited at 250 W: (a) C 1s, (b) O 1s, (c) Sn 3d and (d) In 3d.

of 0.5 wt%. This result is in accordance with the uniformity criteria given for ITO films [28]. This result shows that uniform and well-crystallized nanocrystalline ITO films could be deposited at 250 W rf power at room temperature.

In order to analyze the chemical states of elements present in the surface of ITO films deposited at 250 W, the XPS wide scan and narrow scan spectra of In $3d_{5/2}$, Sn $3d_{5/2}$, O 1s and C 1s were recorded in the binding energy range from 0 to 1100 eV and shown in Figs. 10 and 11, respectively. The binding energy of the O 1s peak is at about 531 eV which can be assigned to the lattice oxygen in In_2O_3 [29]. The In $3d_{5/2}$ peak at 446.98 eV expresses the In^{3+} bonding state from In_2O_3. The peak at 488.9 eV is assigned to the binding energy of Sn $3d_{5/2}$ that corresponds to the Sn^{4+} bonding state in the ITO lattice. The XPS peaks are sharp without peak broadening or splitting which confirms the absence of SnO phase with lower valence Sn^{2+} bonding state. The C 1s peak at 287.0 eV, is related to the surface pollution. These observations show the formation of highly conducting ITO film at 250 W with oxygen bonded to Indium and Indium with In^{3+} and Sn^{4+} bonding states [30]. The composition of Sn and In calculated from XPS is 9.5 and 80.4 wt%, respectively which is comparable with the result of EDX given in Fig. 9.

In order to follow the film growth mechanism, surface morphological studies were conducted for the ITO films using AFM. 3D images have been used for surface quality observation and 2D images with surface scan were used for the evaluation of grain size and surface roughness parameters. Fig. 12 shows the AFM images of the surface morphologies (3×3 μm) of the ITO films deposited at various rf powers. All the films show nano-sized grains and compact microstructure. The morphology of ITO films significantly varied with different rf powers. In the case of ITO films deposited at 50 W, the surface contains a mixture of small grains embedded with in larger agglomerated grains (Fig. 12(a)) confirming its amorphous nature. As the rf power is increased to 250 W, the surface becomes highly uniform with larger grains (Fig. 12(c)). The measured root-mean-square roughness (R_{rms}) is found increasing from 1.7 to 11.5 nm with increasing rf power from 50 to 250 W as shown in Fig. 12(b) and (d), respectively which may be due to the increase in grain size. At 350 W, a decrease in grain size (Fig. 12(e)) and a reduced rms roughness value of 3.2 nm (Fig. 12(f)) is observed. These observations are in accordance with the XRD results presented earlier in Section 3.1.

4. Discussion

The Fig. 1 clearly shows that the ITO films developed to (2 2 2) orientation from amorphous structure with increasing rf power. From thermodynamics point of view, the preferred orientation of a thin film is evolved when a plane acquires the lowest surface energy [31]. The preferential orientation development mainly depends on the initial deposition conditions and (4 0 0) orientation is usually considered to be preferred due to its thermodynamically favorable nature with lowest surface energy. But, the mechanism in ITO film formation by sputtering at room temperature is entirely

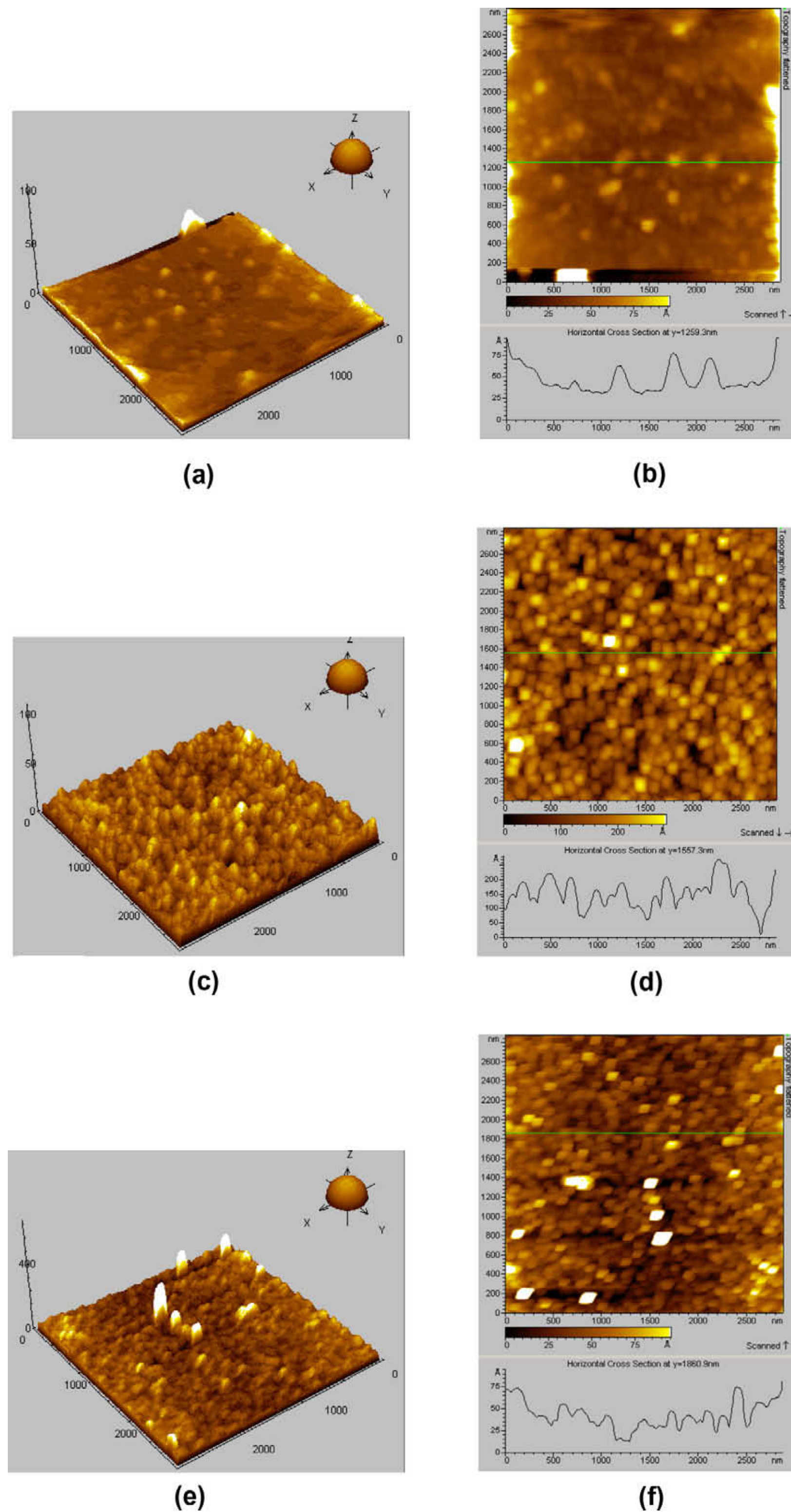

Fig. 12. 3D (a,c,e) and 2D (b,d,f) AFM images of the surface of ITO films deposited at rf power 50 W (a,b), 250 W (c,d) and 350 W (e,f).

different which suggests a two steps growth process with widely varying rf power. As far as rf sputtered ITO films is concerned the fact is that (2 2 2) preferred orientation is invariably dominant during the initial growth stage under any deposition conditions [32]. As soon as sputtering starts, indium atoms reaches the substrate first to initiate nucleation process and settle at the lowest energy (1 1 1) plane which is also the dense packing plane of indium lattice with face-centered tetragonal structure.

In the case of bixbite ITO films, the (2 2 2) plane is the most densely packed plane [33] accompanied with highest energy as well. The variation in the ratio of $I_{(2\,2\,2)}/I_{(4\,0\,0)}$ with sputtering power is shown in Fig. 13. It shows a minimum at 250 W with increasing trend on both sides of lower and higher power density. At lower sputtering power, the energy acquired by the sputtering inert Ar^{+} ions which are colliding on the target may be low due to relatively lower discharge voltage. This results in generating sputtered atoms

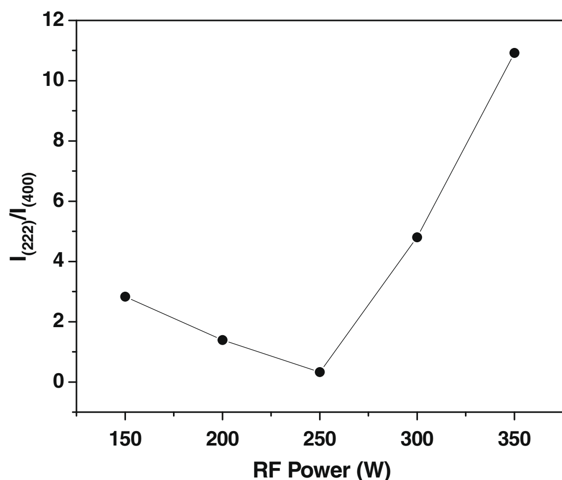

Fig. 13. Variation of the ratio of peak intensity of (2 2 2) and (4 0 0) planes with various rf power.

with low energy. In addition, the energy imparted by ion bombardment will be low due to reduced ion density. Because of these effects, the adatoms mobility is very low at lower sputtering power. Hence, ITO films deposited with 50 and 100 W show amorphous nature. With increasing sputtering power, the density of (2 2 2) oriented grains decreased upto 250 W, and then increased. At the sputtering power 250 W, the ITO films are highly (4 0 0) oriented which elucidates that at this power, the adatoms acquire sufficient activation energy leading to the formation of thermodynamically favorable (4 0 0) planes. The intensity of (4 0 0) peak increased reaching a maximum at 250 W, and then once gain decreased at higher sputtering power. Such a decrease in (4 0 0) peak intensity is attributed to the reduction in the diffusion length of adatoms. At higher sputtering power, due to high density of ions/atoms, the adatoms are piled up and more likely to be buried by the fastly arriving sputtered atoms even well before these adatoms find more kinetically limited (2 2 2) orientation as observed for the ITO films deposited at higher sputtering power here [34].

The lattice constant values of the ITO films deposited at all sputtering powers are greater than the standard value of 10.118 nm for bixbite In_2O_3. This is mainly due to the incorporation of tin as Sn^{4+} in the In^{3+} sites in the In_2O_3 lattice and to the increase in repulsive forces realized from the additional positive charge of the tin atoms. As seen in Fig. 2, lattice constant decreases, but the grain size increases up to a sputtering power of 250 W which reveals an increased crystallinity till the optimum sputtering power and then show opposite trends. Further increase in lattice constant between 250 and 350 W may be due to the removal of oxygen anions from ITO films deposited at higher sputtering energy conditions and the associated repulsive force increase leads to an enlargement of the unit cell [35].

It can be observed from the Fig. 5 that E_g increases with increasing rf power upto 250 W and then decreases which might have been mainly influenced by the varying crystallinity of the ITO films. When the grain size increases the crystallinity also improves, the density of grain boundaries decreases which results in trapping of fewer carriers in the space change region, leading to the generation of higher carrier concentration in the lattice. This causes the Burstein-Moss (BM) shift [22] which can be represented by parabolic band edges as

$$E_g - E_{go} = \Delta E_g^{BM} = \frac{h^2}{8\pi^2 m^*}(3\pi^2 n_e)^{2/3} \quad (8)$$

Where E_{go} in the intrinsic band gap, m^* is the reduced electron effective mass and n_e is the carrier concentration. For ITO films with maximum crystallinity, the BM shift is larger, indicating a higher carrier concentration which shows a higher band gap as well.

The different interaction processes taking place during the different growth stages of the films may induce changes in the band structure of the material. The improvement in the crystalline nature of the films may result in Sn^{4+} substitution more effective and decreases the concentration of donors trapped at the crystalline defects [36].

At constant argon pressure without oxygen, increasing rf power may result in more argon ions which will sputter more Sn + In metal from the target giving more oxygen deficient ITO films. Oxygen deficiency results in a high carrier density as more free electrons are available from oxygen vacancies in the ITO matrix and also from Sn^{4+} ions at In^{3+} substitutional sites [37]. During the initial stages of ITO film formation at low rf power, amorphous films are developed with Sn atoms mostly present in the interstitial regions. As rf power increases, the diffusion of Sn atoms from interstitial regions and grain boundaries into the In cation sites takes place leading to the increase in carrier concentration. When the 4 valence Sn atom replaces trivalent In, one electron is released for conduction. Hence, when rf power is increased to 250 W, the crystallinity of ITO film is improved showing (4 0 0) preferred orientation with enhanced Sn diffusion resulting in higher carrier concentration. However, the increase in band gap from 3.57 eV to 3.69 eV is 0.12 eV only which is low. This may be attributed to the competitive action between the following band gap increasing and reducing phenomena in the lattice. It is observed that the refined crystalline structure would reduce the availability of near band-edge states arising from disorders and effectively increase the observed band gap. At the same time, the increased carrier concentrations may also contribute in decreasing the band gap due to shifts in plasma resonance frequency. For the ITO film deposited at rf powers greater than 250 W, an increase in resistivity along with a decrease in carrier concentration and mobility are observed due to less crystalline nature of the ITO films associated with the changed to (2 2 2) orientation.

The decrease in resistivity as well as the increase in grain size with increasing rf power coincides with an observed increase in grain size of the ITO films prepared with increasing substrate temperature [38]. The larger grains so formed reduce the recombination and scattering of charge carriers at grain boundaries resulting in high carrier mobility in ITO films prepared using an rf power up to 250 W in the present study [39]. The observed rapid reduction in resistivity around 250 W may be also attributed to a transition from amorphous to polycrystalline phase [40]. The surface morphology of ITO films deposited at different rf powers showed different surface nature. As inferred from the AFM pictures, the grain size of the ITO film deposited at 250 W is larger (86 nm) when compared to the films deposited at 50 W (62 nm) and at 350 W (71 nm), respectively. In the AFM image of 50 W power deposited film, there is no evidence of polycrystalline nature, but amorphous, except some aggregated grains protruding on the flat surface layer. The other surfaces show uniform grains revealing their polycrystalline nature but with varying size. R_{rms} value of the ITO film deposited at 250 W is higher than the other films due to its larger grain size.

5. Conclusions

ITO films have been deposited on quartz substrates by rf sputtering at various rf power varying from 50 to 350 W. An amorphous to crystalline transition was observed and the preferential orientation of ITO films also showed a dependence on rf power. The film deposited at 250 W showed (4 0 0) orientation. Growth

mechanism, for the films deposited below and above 250 W, followed the (2 2 2) orientation even when the films showed either amorphous or less crystalline nature. With the increase of rf power, the grain size and crystalline quality of ITO films were improved, the Hall mobility increased to a maximum of 8.3 cm^2/vs and the resistivity decreased to a minimum of $4.3 \times 10^{-3}\ \Omega$ cm. The band gap is 3.69 eV and the refractive index and low extinction coefficient values in the visible region confirms the formation of highly crystalline, void free and compact ITO films whose microstructural parameters like strain and dislocation density are minimum at 250 W. XPS study shows the substitution of In^{3+} sites with Sn^{4+} and EDX result reveals the uniform distribution of In and Sn on the surface supported by the smoother surface with nano grains as observed from AFM pictures. Through these results, it can be confirmed that room temperature ITO films on quartz substrates with $10^{-3}\ \Omega$ cm and above 80% transmittance can be obtained using an rf power of 250 W at room temperature.

References

[1] C.G. Granqvist, A. Hultaker, Thin Solid Films 411 (2002) 1.
[2] H. Kauazoe, M. Yasukawa, H. Hyodo, M. Kunita, H. Yanagi, H. Hosono, Nature 389 (1997) 939.
[3] J.F. Nierengarten, G. Hadziioamnou, N. Armaroli, Mater. Today 4 (2001) 6.
[4] G. Neri, A. Bonavita, G. Micali, G. Rizzo, N. Pinna, M. Niederberger, Thin Solid Films 515 (2007) 8637.
[5] H.L. Hartnagel, A.L. Dawar, A.K. Jain, C. Jagadish, Semiconducting Transparent Thin Films, Institute of Physics, Bristol, 1995.
[6] C.N. Carvalhio, A. Luis, O. Conde, E. Foitunato, G. Lavareda, A. Amaral, J. Non-Cryst. Solids 299–302 (2002) 1208.
[7] J. Herrero, C. Guillen, Vacuum 67 (2002) 611.
[8] S. Ishibashi, Y. Higuchi, Y. Ota, K. Nakamura, J. Vac. Sci. Technol. A 8 (1990) 1399.
[9] C.G. Granquist, Appl. Phys. A 52 (1991) 83.
[10] N.G. Patel, K.K. Makhija, C.J. Panchal, D.B. Dave, V.S. Vaishnav, Sens. Actuators B 23 (1995) 49.
[11] W. Gopel, A.D. Amico, G. Sberveglieri (Eds.), in: Proceedings of the First European School on Sensors (ESS94), World Scientific, 1995, p. 49.
[12] S. Venkatachalam, D. Mangalaraj, Sa.K. Narayandass, Physica B 393 (2007) 47.
[13] E. Terzini, P. Thilakan, C. Minarini, Mater. Sci. Eng. B 77 (2000) 110.
[14] P.K. Song, Y. Shigesato, M. Kamei, Jpn. J. Appl. Phys. 38 (1999) 2921.
[15] H. Iozumi, F.O. Adurodiya, T. Kaneyoshi, T. Ishihara, H. Yoshioka, M. Motoyama, J. Appl. Phys. 91 (2002) 1213.
[16] F.E. Akkad, M. Marafi, A. Punnoose, G. Prahu, Phys. Stat. Sol. 177 (2000) 445.
[17] H.R. Faliah, M. Ghasemi, A. Hassanzadeh, H. Steki, Physica B 383 (2006) 274.
[18] J. George, C.S. Menon, Surf. Coat. Technol. 132 (2000) 45.
[19] S. Ohmo, Y. Kawaguchi, A. Miyamma, Y. Sato, P.K. Song, M. Yoshikawa, P. Frech, Y. Shigesarto, Sci. Technol. Adv. Mater. 7 (2006) 56.
[20] L. Hao, X. Diao, H. Xu, B. Gu, T. Wang, Appl. Surf. Sci. 254 (2008) 3504.
[21] J.R. Rani, V.P. Mahadevan Pillai, R.S. Ajimsha, M.K. Jayaraj, R.S. Jayashree, J. Appl. Phys. 100 (2006) 014302.
[22] E. Burstein, Phys. Rev. 93 (1954) 632.
[23] J.C. Manifacier, M. De Municia, J.P. Fillard, E. Vicario, Thin Solid Films 41 (1977) 127.
[24] R. Swanepoel, J. Phys. E: Sci. Instrum. 17 (1984) 896.
[25] R. Swanepoel, J. Phys. E: Sci. Instrum. 16 (1983) 1214.
[26] R. Das, K. Adhikary, S. Ray, Appl. Surf. Sci. 253 (2007) 6068.
[27] S.J. Hong, J.I. Han, Curr. Appl. Phys. 681 (2006) 206.
[28] S. Seki, Y. Sawada, T. Nishide, Thin Solid Films 338 (2001) 22.
[29] A. Gurlo, N. Barsan, M. Ivanoskaya, U. Weiman, W. Gpel, Sens. Actuators B 47 (1998) 92.
[30] S. Li, X. Qiao, J. Chen, Mater. Chem. Phys. 98 (2006) 144.
[31] R.W. Smith, J. Appl. Phys. 81 (1997) 1196.
[32] Y.S. Jung, S.S. Lee, J. Cryst. Growth 259 (2003) 343.
[33] C.H. Yi, I. Yasui, Y. Shigesato, Jpn. J. Appl. Phys. 34 (1995) 1638.
[34] H. Kim, J.S. Horwitz, G. Kushto, A. Pique, Z.H. Kafafi, C.M. Gilmore, D.B. Chrisey, J. Appl. Phys. 88 (2000) 6021.
[35] G.G. Gonzalez, J.B. Cohen, J.H. Hwang, T.O. Mason, J. Appl. Phys. 87 (2001) 2550.
[36] L.J. Meng, A. Macarico, R. Martins, Vacuum 46 (1995) 673.
[37] V. Teixeina, H.N. Cui, L.J. Meng, E. Fortunato, R. Mathins, Thin Solid Films 420–421 (2002) 70.
[38] S. Calnan, H.M. Upadhaya, M.J. Thwaites, A.N. Tiwari, Thin Solid Films 515 (2007) 6045.
[39] J. Lee, H. Jung, D. Lim, K. Yang, W. Song, J. Li, Thin Solid Films 480–481 (2005) 157.
[40] Y.S. Jung, D.W. Lee, D.Y. Jeon, Appl. Surf. Sci. 221 (2004) 136.